Combustion and Flame 156 (2009) 1755–1763

Contents lists available at ScienceDirect

Combustion and Flame

journal homepage: www.elsevier.com/locate/combustflame

# On the influence of the char gasification reactions on NO formation in flameless coal combustion

Hannes Stadler *, Dobrin Toporov, Malte Förster, Reinhold Kneer

*Institute of Heat and Mass Transfer, RWTH Aachen University, Eilfschornsteinstraße 18, 52056 Aachen, Germany*

ARTICLE INFO

*Article history:*
Received 4 December 2008
Received in revised form 12 May 2009
Accepted 9 June 2009
Available online 7 July 2009

*Keywords:*
Flameless combustion
Coal combustion
Char gasification
Simulation

ABSTRACT

Flameless combustion is a well known measure to reduce $NO_x$ emissions in gas combustion but has not yet been fully adapted to pulverised coal combustion. Numerical predictions can provide detailed information on the combustion process thus playing a significant role in understanding the basic mechanisms for pollutant formation. In simulations of conventional pulverised coal combustion the gasification by $CO_2$ or $H_2O$ is usually omitted since its overall contribution to char oxidation is negligible compared to the oxidation with $O_2$. In flameless combustion, however, due to the strong recirculation of hot combustion products, primarily $CO_2$ and $H_2O$, and the thereby reduced concentration of $O_2$ in the reaction zone the local partial pressures of $CO_2$ and $H_2O$ become significantly higher than that for $O_2$. Therefore, the char reaction with $CO_2$ and $H_2O$ is being reconsidered. This paper presents a numerical study on the importance of these reactions on pollutant formation in flameless combustion. The numerical models used have been validated against experimental data. By varying the wall temperature and the burner excess air ratio, different cases have been investigated and the impact of considering gasification on the prediction of NO formation has been assessed. It was found that within the investigated ranges of these parameters the fraction of char being gasified increases up to 35%. This leads to changes in the local gas composition, primarily CO distribution, which in turn influences NO formation predictions. Considering gasification the prediction of NO emission is up to 40% lower than the predicted emissions without gasification reactions being taken into account.



## 1. Introduction

Flameless combustion is of ever growing interest as a measure to reduce $NO_x$ emissions from combustion processes. It is state of the art for gas burners in the heat treatment industry. Here, $NO_x$ emissions are near the detection limit. In flameless combustion the reaction zone is extended throughout a large volume of the furnace. Thus, flame formation with its inherent high temperature peaks is inhibited and the temperature field and species distribution are more homogeneous. This combustion mode is achieved by a strong recirculation of flue gases to the primary reaction zone causing the reactants to be significantly diluted. Recently, there is an increased interest in applying this technique to pulverised coal combustion. It has already been shown experimentally that $NO_x$ emissions of coal combustion could be significantly reduced with such a burner design [1,2].

In conventional flames the oxygen concentration in the reaction zone is high enough for most of the char to be oxidised by oxygen. This reaction is several orders of magnitude faster than the reactions with carbon dioxide and water vapour. Therefore, the gasification reactions are often neglected in numerical investigations, [3–7].

In flameless combustion, however, the intense recirculation of hot combustion products causes fast dilution of the $O_2$ in the reaction zone. Thus, the partial pressure of $CO_2$ and $H_2O$ become higher than that of $O_2$ and therefore the oxidation of char is likely to follow diverse paths in parallel. Considering this in numerical simulations should lead to more accurate predictions of gas species concentrations. The need for more detailed models for char burnout was recently reported by Schaffel et al. [8].

The importance of consideration of the gasification reactions was already observed for a standard low $NO_x$ burner [9]. In order to identify the boundary conditions under which gasification reactions should be considered and to get a better understanding of the pollutant formation mechanisms in flameless coal combustion, a numeric parameter study was carried out to determine the relative importance of oxygen, carbon dioxide and water vapour as oxidiser for char and the influence of the changed temperature field and species concentration on NO formation.

## 2. Experimental setup

Experiments were conducted in a vertical, cylindrical, top fired furnace with a diameter of 400 mm and a total length of 4200 mm, Fig. 1. In this furnace the burner is axially traversable allowing for

* Corresponding author.
*E-mail address:* stadler@wsa.rwth-aachen.de (H. Stadler).

0010-2180/$ - see front matter © 2009 The Combustion Institute. Published by Elsevier Inc. All rights reserved.
doi:10.1016/j.combustflame.2009.06.006

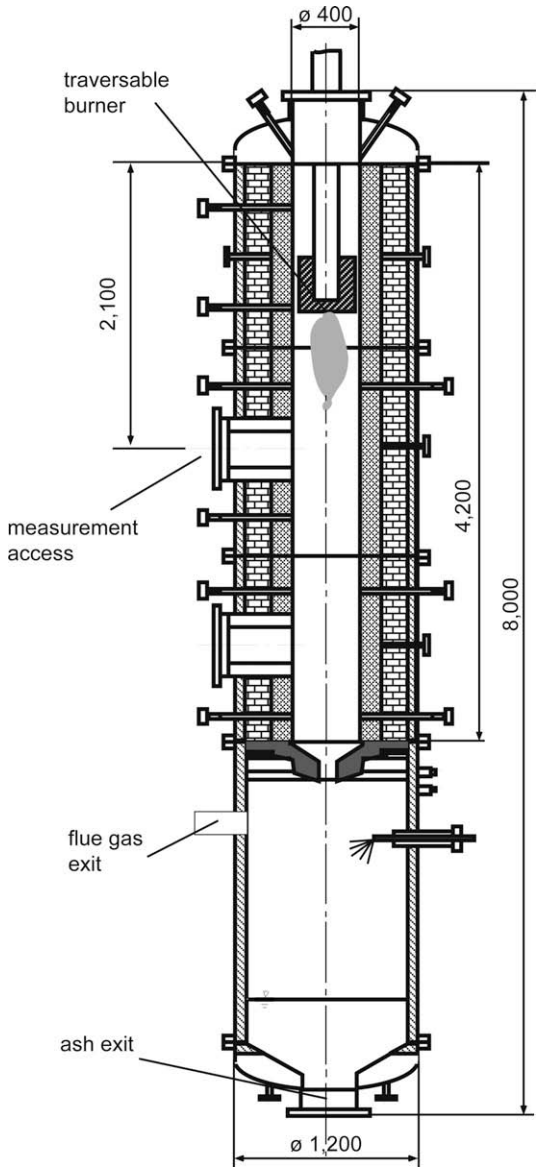


**Fig. 1.** Test facility, all dimensions in (mm).

measurements at different distances from the burner through a single measurement plane. Thus, for measurements of the velocity the furnace is only 2100 mm plus the actual distance of the measurement plane from the burner whereas global measurements were carried out with a total furnace length of 3900 mm. During in flame measurements burnout air was introduced 700 mm from the bottom of the furnace, whereas during global measurements it was introduced at the measurement plane with the burner 1800 mm above the measurement plane. Electrical heating was used for regulation of the wall temperature.

The pulverised coal burner employed in this study, Fig. 2, was developed according to the design of flameless gas burners. The predominant design criterion for a flameless combustion burner is the avoidance of high temperature zones in order to reduce the formation of thermal NO. In coal flames thermal NO makes up only a small fraction of the total NO emission as fuel NO accounts for a major portion of NO emissions. However, experiments [2] have shown the high NO reduction potential of flameless coal combustion which cannot be attributed to the prevention of thermal NO alone. In accordance with gas burners for flameless combustion a homogeneous temperature distribution is achieved by good mixing of the incoming fresh mixture and the flue gas. A high inlet momentum of the secondary air is used to induce the required recirculation of the flue gas which is then entrained into the inlet streams.

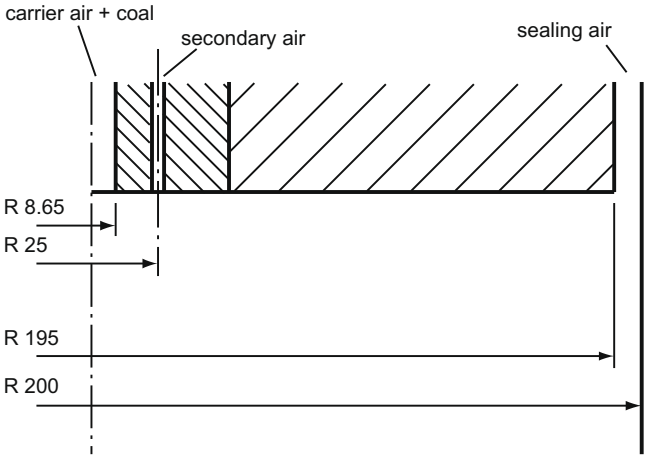


**Fig. 2.** Sketch of burner design, all dimensions in (mm).

The dimensions of the investigated burner are given in Fig. 2. The coal is transported by a carrier air flow and enters the chamber through a central inlet. The secondary air is injected through three nozzles (diameter 4.2 mm) which are arranged annularly around the central coal jet. A sealing air stream was used in the gap between the traversable burner and the furnace wall in order to prevent particles from entering the volume above the burner. For the calculation of the burner excess air ratio this air stream is also considered.

This burner design was subject to an experimental study investigating its performance with different coals and different stoichiometric boundary conditions [2]. The arrangement of the nozzles allows recirculated hot flue gases to penetrate between the air jets directly to the coal jet. Thus, the secondary air as well as the coal are diluted with flue gas before they mix. The oxygen concentration in the reacting mixture is reduced and thus the peak flame temperature is lowered.

Furthermore, it can be expected that NO that is produced in the reaction zone is partially recirculated together with the flue gases thus allowing for NO reduction in the burner vicinity.

For the current numerical investigation reference data from three different experiments were considered. The boundary conditions are listed in Table 1. The first case at a burner excess air ratio of 0.7 was used to verify the flow field as data from velocity measurements were available for comparison. The other two cases (burner excess air ratios 0.8 and 0.9) were used for validation of NO predictions.

The investigated coal is a blend from different Polish bituminous coals. Proximate and ultimate analysis are given in Table 2.

### 2.1. Measurement technique

Velocity measurements were carried out using Laser Doppler Anemometry (LDA). The Laser Doppler Anemometry permits non-intrusive measurements of axial and tangential velocities with high spatial and temporal resolution.

For measurements within the coal flame no additional seeding of the flow was necessary since the particle density of coal and ash particles is sufficient within the whole measurement volume. Due to the small particle size (90% of the coal mass is contained in particles smaller than 75 μm; $D_{p90} < 75$ μm) it can be assumed

**Table 1**
Flow boundary conditions and NO emissions determined from experiments.

| Burner EAR* | Coal flow $\left(\frac{kg}{s}\right)$ | Carrier air $\left(\frac{kg}{s}\right)$ | Secondary air $\left(\frac{kg}{s}\right)$ | Sealing air $\left(\frac{kg}{s}\right)$ | Burnout air $\left(\frac{kg}{s}\right)$ | Wall temperature (°C) | Global NO emission (ppm) |
|---|---|---|---|---|---|---|---|
| 0.7 | $1.167 \times 10^{-3}$ | $3.389 \times 10^{-3}$ | $3.699 \times 10^{-3}$ | $2.730 \times 10^{-3}$ | $8.800 \times 10^{-3}$ | 900 | 50 |
| 0.8 | $1.167 \times 10^{-3}$ | $3.389 \times 10^{-3}$ | $4.561 \times 10^{-3}$ | $2.766 \times 10^{-3}$ | $6.824 \times 10^{-3}$ | 900 | 190 |
| 0.9 | $1.167 \times 10^{-3}$ | $3.389 \times 10^{-3}$ | $5.783 \times 10^{-3}$ | $2.766 \times 10^{-3}$ | $5.388 \times 10^{-3}$ | 900 | 261 |

* EAR: excess air ratio.

**Table 2**
Proximate and ultimate analysis in (mass%) of bituminous coal blend.

| Proximate analysis | | Ultimate analysis | |
|---|---|---|---|
| Water | 0.60 | C | 85.90 |
| Ash | 3.60 | H | 5.09 |
| Volatiles | 33.00 | O | 2.94 |
| Char | 62.80 | N | 1.41 |
| | | S | 0.46 |

that the slip between particles and gas is negligible so that measured particle velocities directly reflect gas velocity [10].

The optical access at the furnace used for the experiments requires a large working distance between the optics and the measurement position within the flow. Therefore, individual beam optics with single beam adjustment are used as transmitting optics. Hence, by increasing the beam distance, an angle of 3.2° could be retained so that a reasonable small measurement volume of 150 μm diameter and 2.5 mm length can be obtained. In order to reduce the effort of alignment, a back scattering setup is chosen where the transmitting and receiving optics are mounted on a single frame. The absolute values of the individual particle velocities are subject to a maximum error of 3% due to an uncertainty in the determination of the actual beam angle in the optical setup.

The velocities reported here are arithmetic mean velocities of the recorded individual particles. Also a 95% confidence interval for the calculated mean is given.

Another uncertainty next to the determination of the velocity lies in the identification of the exact measurement position. The axial positioning of the burner occurs with an uncertainty of 1 mm. Also the radial positioning of the optical system relative to the furnace axis underlies an uncertainty of approximately 5 mm.

## 3. Numerical models

Numerical simulations of pulverised coal combustion were carried out using the CFD code Fluent 6.3.26 with modified (UDF-based) devolatilisation, char oxidation and gas phase combustion submodels. The flow field was solved using the k-$\varepsilon$-realisable turbulence model with the Simple algorithm for velocity–pressure coupling. Transport equations for the mass fractions of seven different gas species (volatiles ($C_xH_yO_lS_nN_m$), water vapour, carbon monoxide, carbon dioxide, sulphur dioxide, oxygen and hydrogen) were calculated with source terms defined according to the reaction scheme proposed below. Being the most abundant species in the gas mixture, the nitrogen mass fraction was calculated from a mass balance. The following kinetic mechanism according to Toporov et al. [11] was assumed for the combustion of volatiles:

$$C_xH_yO_lS_nN_m + \left(\frac{x}{2} + n - \frac{l}{2}\right)O_2 \rightarrow xCO + \frac{y}{2}H_2 + nSO_2 + \frac{m}{2}N_2 \quad (1)$$

and subsequently:

$$CO + \frac{1}{2}O_2 \rightarrow CO_2 \quad (2)$$

$$H_2 + \frac{1}{2}O_2 \rightarrow H_2O \quad (3)$$

The interaction between the turbulence and chemical reactions in the gas phase was modelled using the Eddy Dissipation Concept model according to Magnussen [12], implemented and presented by Heil et al. [13] with kinetic rates given in Table 3.

Coal particle combustion was simulated based on a stochastic Lagrangian procedure to track the particle trajectories in the flow field. The coal particle undergoes decomposition into char and volatile material. The volatile material is assumed to rapidly form CO, reaction (1), from which subsequently $CO_2$ is formed, reaction (2), whereas the char is oxidised in the later stages of combustion.

The devolatilisation process was modelled using a single reaction approach with an activation energy of 74 kJ/(mol K).

For heterogenous oxidation of char two different mechanisms have been employed. The first mechanism implies only partial char oxidation by oxygen:

$$C_{char} + \frac{1}{2}O_2 \rightarrow CO \quad (4)$$

Simulations with this simple mechanism were used as comparison for the investigation of the influence of the gasification reactions. The second mechanism also implies partial char oxidation by oxygen according to reaction (4) but extends further by considering char gasification by $CO_2$ and $H_2O$. For modeling purposes the reaction of coal char with $CO_2$ and $H_2O$ may be simplified as the reaction of carbon with $CO_2$ and $H_2O$, respectively:

$$C_{char} + CO_2 \rightarrow 2CO \quad (5)$$

$$C_{char} + H_2O \rightarrow CO + H_2 \quad (6)$$

The Arrhenius coefficients used for these reactions are given in Table 4. For reactions (4)–(6) first order was considered.

However, one should bear in mind that although carbon is the dominant atomic species present in coal char, its reactivity can be quite different from that of the actual char. Gasification rates for a number of coals and chars at varying boundary conditions are available in literature [17–21]. Often coal is more reactive than pure carbon for a number of reasons. In coal char various reactive organic functional groups can enhance its reactivity as well as naturally occurring mineral ingredients which enhance reactivity catalytically. The actual reactivity also changes in time with advancing burnout [22]. As no experimental data are available for the coal investigated in this study, the rates for graphite were used which in most cases are rather conservative.

Rates given in Table 4 are limited in the temperature range. For temperatures out of the given range coefficients valid for the nearest regime were taken.

**Table 3**
Kinetic rates of gas reaction, units are $m^3$ kmol s J K.

| Reaction | $A$ | $E$ | Ref. |
|---|---|---|---|
| (1) | $1.1787 \times 10^7$ | $5.56 \times 10^7$ | Shaw et al. [14] |
| (2) | $1.3 \times 10^{11}$ | $1.26 \times 10^8$ | Howard et al. [15] |
| (3) | $9.87 \times 10^8$ | $3.1 \times 10^7$ | Hsu and Jemcov [16] |

**Table 4**
Arrhenius coefficients for heterogeneous reactions.

| Reaction | Carbon type | $A_a\left(\frac{1}{s}\right)$ | $E_a/R$ (K) | Temperature range (°C) | Ref. |
|---|---|---|---|---|---|
| (4) | Char | $5 \times 10^{-3}$ | 8900 | 677–1377 | Field [23] |
| (5) | Graphite | $1.35 \times 10^{-4}$ | 16,300 | 850–950 | Smoot and Pratt [24] |
| | Graphite | $6.35 \times 10^{-3}$ | 19,500 | 950–1400 | |
| (6) | Graphite | $3.19 \times 10^{-1}$ | 25,020 | 860–960 | Smoot and Pratt [24] |
| | Graphite | $1.92 \times 10^{-3}$ | 17,680 | 1000–1160 | |

Pulverised coal combustion was modelled with water evaporation, devolatilisation and char-burnout submodels calculated in parallel.

The radiative heat source was calculated as a function of the local irradiation, calculated by the Discrete Ordinates radiation model. The local absorption coefficient was calculated as the sum of the particle and gas absorption coefficients. The latter was based on the Weighted Sum of Grey Gases model which considers the absorption coefficients of different grey gases of the mixture.

The three dimensional computational domain represents 1/6 of the furnace volume with symmetric boundary conditions. The numerical grid contains 370,000 cells. The emissivities of the furnace and burner walls were taken to be $\varepsilon = 0.7$ and $\varepsilon = 0.3$, respectively.

In flow conditions were determined with a preceding simulation of the burner pipe flow. Thus, boundary conditions for velocity and temperature distribution across the inlet were obtained.

## 4. Validation of simulations with experiments

Data from LDA velocity measurements were used to verify the inlet boundary conditions of the numerical simulation. Measurements had been carried out at several planes 25 mm, 50 mm, 75 mm and 100 mm from the burner. On these planes radial profiles were taken. The line of measurements was inclined to the axis from the primary air to the secondary air jet by about 16°. Thus, no data from within the secondary air jet in burner vicinity is available.

In Fig. 3 experimental and numerical data are compared. At a distance of 25 mm from the burner (uppermost graph) the experimental data reflects the central carrier air/coal jet with a maximum velocity of around 21 m/s. The secondary air does not extend to the line of measurements at this plane. Yet, a minor influence of the secondary air jet can be seen in the simulation. This difference might be due to the uncertainty in axial positioning of the burner described above.

At a distance of 50 mm (second from top in Fig. 3) the secondary air jet has spread far enough to be detected along the line of measurements. It appears as a second peak at a radial distance of 20 mm from the axis. Its maximum velocity is about 16 m/s. The measured minimum between the peaks is not as low as in the numerical simulation which is due to a lower resolution of the experiments and the length of the measurement volume of about 2.5 mm. Data from within this measurement volume is integrated so that structures smaller than its length cannot be fully resolved. Qualitatively, data from the planes at 75 and 100 mm (lower two graphs in Fig. 3) look the same, only peak values differ slightly. The maximum velocities are underpredicted by about 3 m/s. The value of the local minimum observed in between the two jets increases with increasing axial distance as the two jets merge. Experimental and numerical data agree well except for an offset of the experimental data of approximately 5 mm. This offset is due to a minor misalignment of the optical system.

The agreement obtained between experimental and numerical data shows that the chosen k-$\varepsilon$-realisable turbulence model and the related inlet boundary conditions are appropriate for the investigated flameless pulverised coal combustion. Therefore, this case was used as a basis for a case-study based investigation of the influence of gasification reactions on NO emission predictions.

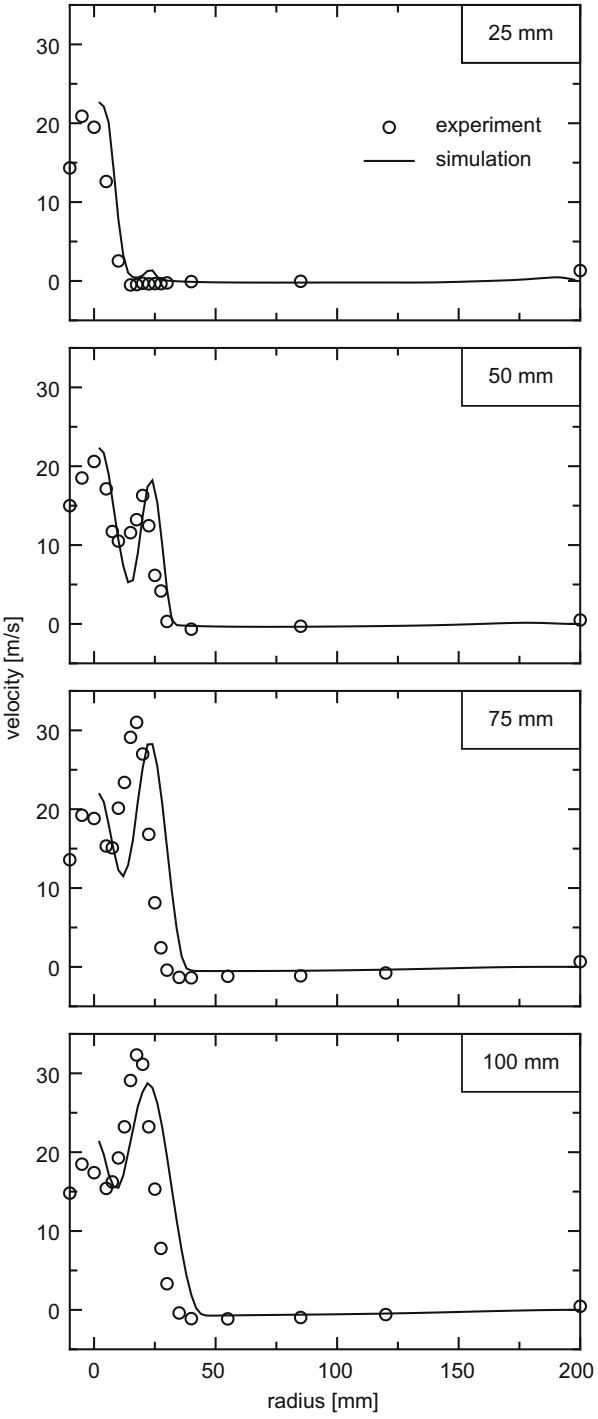


**Fig. 3.** Comparison of experimental and numerical data at distances of 25–100 mm from the burner.

### 4.1. $NO_x$-models

Standard FLUENT NO-postprocessing models considering thermal NO, prompt NO, fuel NO formation and NO reburning with volatiles were used. Thermal NO was calculated according to the extended Zeldovich mechanism with a partial equilibrium approach for the radicals O and OH. For prompt NO volatiles were considered the fuel species.

One third of the total fuel nitrogen is assumed to be released with the volatiles and the remaining two thirds are released together with the char burnout since the volatiles make up about one third of the coal mass and the char makes up two thirds of the coal mass. For both pathways the same proportioning of the intermediates was chosen. It was assumed that 60% of the nitrogen are released via the intermediate HCN and 10% via the intermediate $NH_3$. The remaining nitrogen is released directly as NO. Reactions considered for NO formation and those leading to the reduction of NO are the following:

$$HCN + O_2 \rightarrow NO + \cdots \quad (7)$$

$$HCN + NO \rightarrow N_2 + \cdots \quad (8)$$

$$NH_3 + O_2 \rightarrow NO + \cdots \quad (9)$$

$$NH_3 + NO \rightarrow N_2 + \cdots \quad (10)$$

The $N_2O$ path has been completely omitted since preliminary simulations showed its influence to be insignificant throughout the range of parameters relevant to this study.

In the temperature range between 1300 °C and 1800 °C NO reburning with volatiles was incorporated. A partial equilibrium approach was considered for the reburning species. The volatiles have a C/H ratio of approximately 2.6. Therefore, $CH_3$ was considered the equivalent reburn fuel.

These parameters were validated against global NO emissions measured during two different experiments at a wall temperature of 900 °C and a burner excess air ratio (EAR) of 0.8 and 0.9, Table 5. Predictions at a burner excess air ratio of 0.8 correspond very well with experimental data, at a burner excess air ratio of 0.9 NO emissions are slightly underpredicted.

## 5. Results and discussion

A number of simulations has been carried out with the wall temperature set between 900 °C and 1500 °C and at burner excess air ratios between 0.7 and 0.9 as listed in Table 6.

The key features of flameless combustion are well resolved. The intense recirculation causes the $O_2$ concentration in the reaction zone to be lower than the $CO_2$ concentration. This high dilution is considered favourable for low $NO_x$ combustion. Fig. 4 shows the predicted temperature distribution with and without gasification reactions at a burner excess air ratio of 0.9 and a wall temperature of 1500 °C. The temperature throughout the whole combustion zone is characterised by small gradients and low peak temperatures compared to the wall or outlet temperature. The predictions show that the gas temperature distribution is independent of the chosen char oxidation model and it is homogeneous in the primary combustion zone. The difference in the obtained maximum temperatures between the different cases does not exceed 20°.

**Table 5**
NO emission in experiments compared to numerical predictions.

| Burner EAR | 0.8 (ppm) | 0.9 (ppm) |
|---|---|---|
| Experiment | 190 | 261 |
| Simulation | 190 | 234 |

**Table 6**
Boundary conditions investigated.

| Burner EAR | Wall temperature (°C) | | | | | |
|---|---|---|---|---|---|---|
| 0.7 | 900 | 1100 | 1200 | 1300 | 1400 | 1500 |
| 0.8 | 900 | | | | | |
| 0.9 | 900 | 1100 | 1200 | 1300 | 1400 | 1500 |

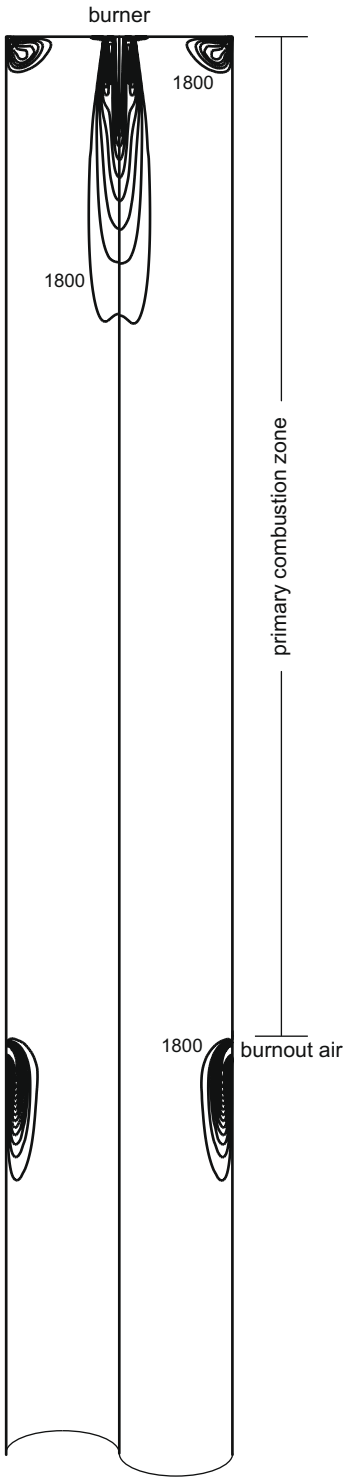


**Fig. 4.** Temperature distribution in the furnace as simulated without gasification reactions (left) and with gasification reactions (right) at a burner excess air ratio of 0.9 and a wall temperature of 1500 °C.

However, within this study it was found that the char gasification reactions can have significant influence on overall char oxidation. Figs. 5 and 6 show the share of CO production from the three reactions considered for char oxidation at a burner excess air ratio of 0.7 (Fig. 5) and 0.9 (Fig. 6), predicted at different wall temperatures. An increase in temperature increases the fraction of char being gasified. At a wall temperature of 1500 °C and a burner excess air ratio of 0.7 up to 30% of the char are gasified by $CO_2$ according to reaction (5) and up to 5% are gasified by $H_2O$, reaction (6). At a burner excess air ratio of 0.9 up to 20% are gasified by $CO_2$ and 3% by $H_2O$. At a given wall temperature the fraction of char being gasified by $CO_2$ or $H_2O$ at a burner excess air ratio of 0.7 is always higher than at a burner excess air ratio of 0.9. It shows that the $O_2$ concentration is the second parameter influencing the rates of gasification. At lower local $O_2$ concentrations a bigger part of the char is gasified.

For the given reaction rates for graphite (Table 4) the reaction of $CO_2$ always yields about 5–10 times as much CO as the reaction with $H_2O$.

The gasification reactions can change the species concentrations significantly. With gasification reactions a bigger portion of the char is oxidised resulting in higher CO concentrations in the primary combustion zone before staging air injection. Since the CO concentration is increased, oxygen is more rapidly being consumed by means of reaction (2). This in turn reduces the oxygen concentration in the substoichiometric zone further. At the lowest investigated temperatures (900 °C) and at a burner excess air ratio of 0.9 the maximum CO concentration obtained in simulations with gasification reactions is about 10% higher than in the case without. Fig. 7 shows the CO distribution at a wall temperature of 1500 °C on the left side as simulated without gasification reactions and on the right side with consideration of the gasification reactions. Here, the obtained maximum CO concentration in simulations with

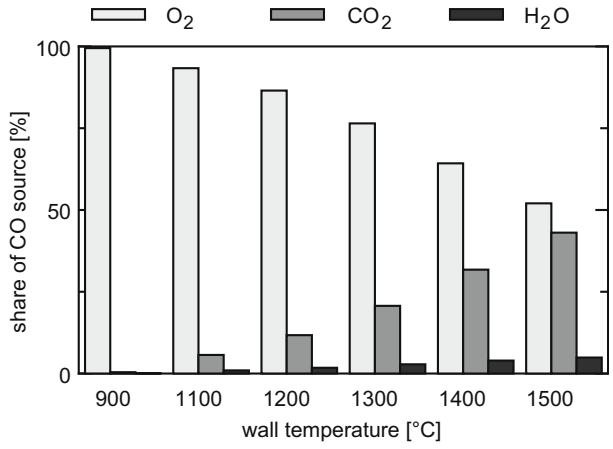


**Fig. 5.** Relative importance of gasification reactions as CO source at burner excess air ratio of 0.7.

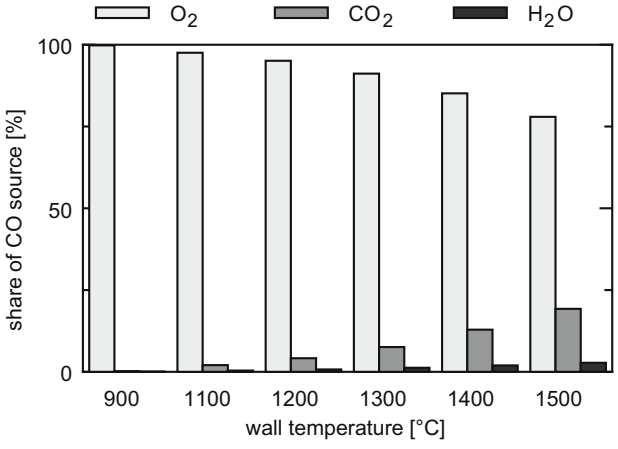


**Fig. 6.** Relative importance of gasification reactions as CO source at burner excess air ratio of 0.9.

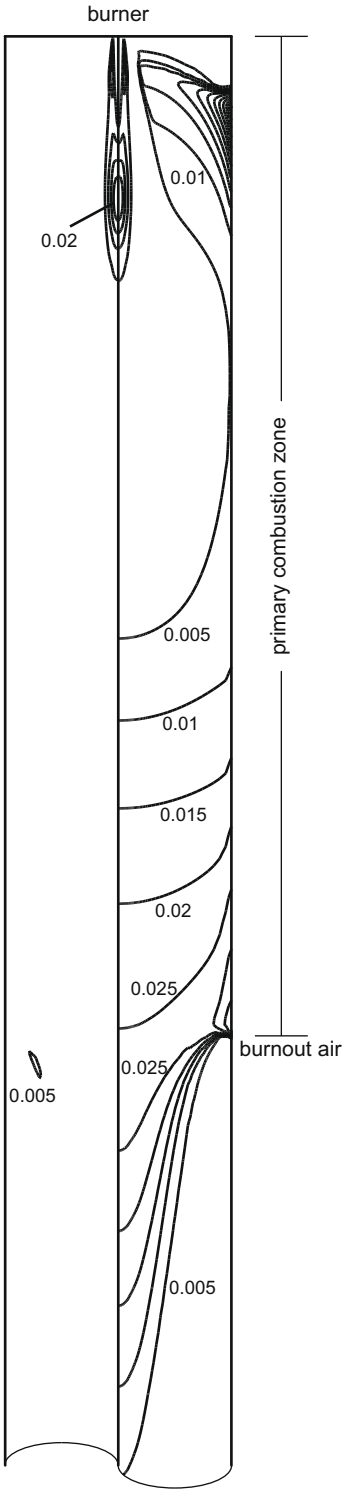


**Fig. 7.** Distribution of mass fraction of CO in the furnace as simulated without gasification reactions (left) and with gasification reactions (right) at a burner excess air ratio of 0.9 and a wall temperature of 1500 °C.

gasification reactions is about twice as high as in the case without. The volume with high CO concentration is enlarged from a localised zone near the burner to the whole primary combustion zone up to the injection of the staging air. In the simulation without gasification reactions (left) high values show up only in the burner vicinity where the volatiles are burned. The CO distribution as simulated with gasification reactions (on the right) features this same peak but, as all oxygen is consumed for the oxidation of CO, the CO concentration starts increasing up to the inlet of the staging air. The path of the recirculation also becomes obvious as a zone of high CO concentration. It extends along the wall up to the inlet of the sealing air where the CO is oxidised. Thus, a major portion of the recirculation occurs in a highly reducing atmosphere favouring low NO production.

This in turn has an influence on the prediction of pollutant formation. As the oxygen concentration decreases, the concentrations of the NO-intermediate products HCN and $NH_3$ increase because reactions (7) and (9) are impeded. The oxygen is more rapidly consumed for CO oxidation (2) as for the oxidation of the intermediates. The increased intermediate concentration in turn leads to higher reaction rates for the reduction routes, reactions (8) and (10) resulting in a lower NO concentration.

An accurate prediction of the CO distribution becomes even more important when its influence on the radical pool is considered. According to Brouwer et al. [25] and Kristensen et al. [26] under selective non catalytic reduction (SNCR) conditions a high CO concentration is beneficial for the reduction of NO because it enlarges the radical pool by its reaction with OH yielding $CO_2$ and H and subsequent chainbranching reactions of H. Under conditions of flameless coal combustion a similar influence of high CO concentration might exist but further work is needed for clarification. With the global models used in this study this effect was omitted.

### 5.1. Results from NO simulations

Fig. 8a shows the calculated global NO emissions at different wall temperatures for both cases – with and without gasification reactions. For a burner excess air ratio of 0.9 NO emission drops continuously with increasing wall temperature up to a wall temperature of 1300 °C. At higher temperatures a strong increase in NO emissions can be seen. For a burner excess air ratio of 0.7 the trend is not so obvious. Between 900 °C and 1100 °C the NO emission increases and drops again towards 1400 °C. A further temperature increase leads to an increased NO emission again. This behaviour is the sum of the individual mechanisms and can be explained when the origin of NO is considered.

Fig. 8b shows the NO produced via the fuel-NO path. The NO models used for the current analysis capture the trend of lower fuel-NO production at higher temperatures as it was reported in several experimental studies [2,27,28]. With higher temperatures less fuel-NO is produced because the reaction of the intermediates HCN and $NH_3$ with NO to form $N_2$, reactions (8) and (10), are faster than the oxidation reactions (7) and (9) especially since the fuel is released in a highly substoichiometric region. This difference becomes more significant with increased temperature.

At temperatures above 1300 °C the predicted fuel-NO emission increases. This effect is due to the exponential increase of reaction rates with temperature but does not necessarily reflect real behaviour as the rate coefficients used do not cover this high temperature range. Similar predictions and comparison with experimental data have been obtained by Alzueta et al. [29].

Fig. 8c shows the contribution of the reburning reactions. The magnitude of the reburning rates is of the same order as the fuel-NO production compensating for most of the production. However, with increasing temperature the amount of NO that is reburned is reduced and seems to stagnate between 1200 °C and 1500 °C causing the overall emission of NO to rise with temperature. A possible reason for the stagnation is that the volatiles, which are considered the reburning species in the current investigation, are consumed faster at higher temperatures so that the slower reaction with NO is impeded.

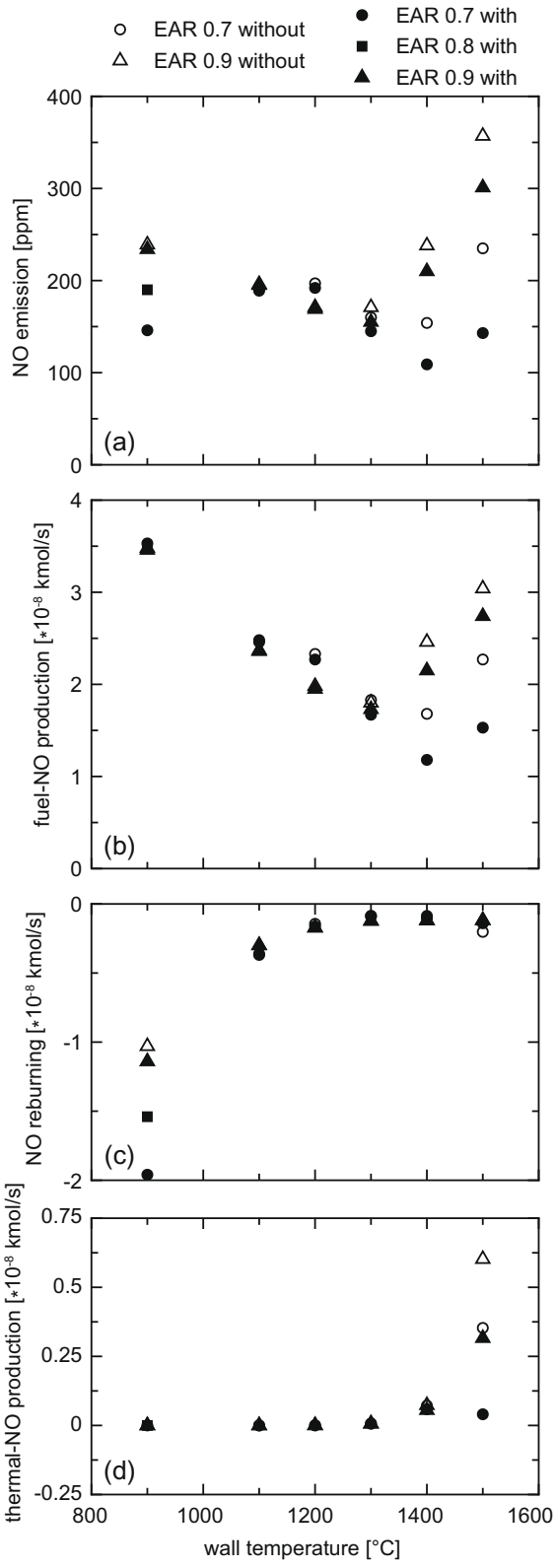


**Fig. 8.** Total predicted NO emission and distribution among mechanisms of NO production and reduction.

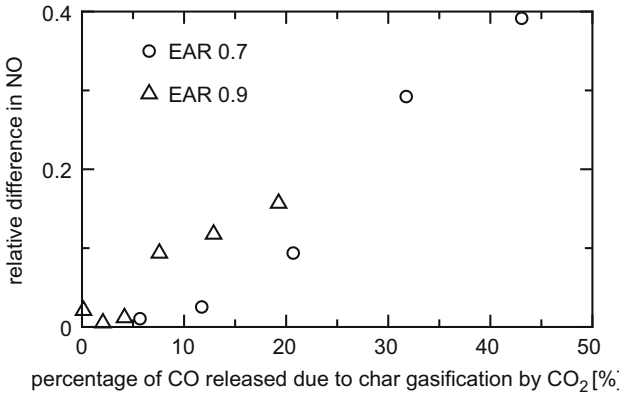


**Fig. 9.** Relative difference of NO emission with and without gasification reactions $\frac{NO_{wo}-NO_w}{NO_{wo}}$ ($NO_{wo}$: predicted NO emission without gasification reactions, $NO_w$: predicted NO emission with gasification reactions) over share of oxidation by $CO_2$ gasification reaction.

Fig. 8d shows the NO production via the thermal path. Up to 1400 °C the overall production is negligible compared to fuel-NO production (less than 5%). This is a direct influence of the flameless combustion mode where peak temperatures are kept low and thus thermal NO formation is reduced. At a wall temperature of 1500 °C a considerable amount of NO is produced via the thermal NO mechanism, however NO formation via the fuel-NO path yields about five times as much NO. In experiments in a similar furnace [2] but with a different coal (lignite instead of bituminous coal) it was found that about one third of total NO emissions in flameless combustion are produced via the thermal NO mechanism at a wall temperature of 1300 °C.

Mancini et al. [30] reported that the prompt NO route is dominant in the fuel rich primary reaction zone of flameless combustion of gaseous fuels, however, the NO mechanism used in the current study showed only a negligible contribution throughout the whole temperature range investigated.

Calculated NO values without gasification reactions are always higher than in the case when the gasification reactions are considered. This is in accordance with Yamamoto et al. [9]. The difference increases with temperature and decreases with the burner excess air ratio. In Fig. 9 the difference in NO prediction is plotted against the share of $CO_2$ gasification reaction in total char oxidation. This figure points up the influence of the gasification reactions on NO prediction. Up to 5% oxidation of char by $CO_2$ the difference of the NO prediction between the simulation with and without gasification reaction is negligible. In this case the species concentrations do not differ significantly. At an increased gasification fraction of 7.5% there is already a 10% difference between the predictions. This difference increases to about 40% at a level of around 45% gasification of the char by $CO_2$.

## 6. Conclusions

A numerical investigation on the influence of char gasification reactions on NO emission predictions has been made. The numerical model has been validated against in-flame measurements of the velocity and global NO emission measurements. A case study approach was used for the assessment of the relative importance of gasification reactions. The wall temperatures assumed in this study were extended beyond those values applicable to standard combustion systems in order to capture the trend. However, the char reactivity strongly depends on the coal type and results observed at high temperatures in this study are likely to be observable at lower temperatures for coals which are more reactive than the graphite underlying the current study.

The use of kinetic data for carbon burnout that is derived for the coal investigated in numerical simulations will lead to quantitative improvements of the predictions.

This work has shown that in flameless pulverised coal combustion a non negligible portion of char can be oxidised by $CO_2$ and $H_2O$. Considering these reactions in simulations of flameless combustion has negligible influence on the predicted temperature distribution but results in different species concentration fields. Hence, the prediction of pollutant formation can alter significantly. In particular the findings are as following:

1. The fraction of char oxidised by $CO_2$ and $H_2O$ increases with temperature and decreases with higher burner excess air ratio.
2. Gasification reactions increase the burnout in the primary combustion zone.
3. $CO_2$ and $H_2O$ gasification lead to an increased CO concentration in the primary combustion zone thus further reducing the $O_2$ concentration.
4. The reduced oxygen concentration leads to a decrease of the concentration of NO intermediate species in the primary reaction zone.
5. Less oxygen and higher NO-intermediate concentrations result in higher reduction of NO.

Based on these observations it can be concluded that the design of a flameless coal combustion burner should promote intense mixing of recirculated hot combustion products and incoming fresh reactants thus allowing simultaneous fast $O_2$ dilution and fuel heat-up which as a result favours char gasification with the benefit of enhanced NO reduction. This design also leads to a homogeneous temperature distribution which is considered advantageous for reduced thermal NO formation.

Although the NO model used in this study was able to capture the correct trend and provide reasonable predictions, a more sophisticated NO model could give more accurate predictions. However, the most recent NO models available in literature have not yet been tested and validated for flameless coal combustion. Thus, the findings from this work can be used as a basis for validation of newer NO models for flameless coal combustion.

## Acknowledgment

The authors gratefully acknowledge the financial support from the European Commission which supported this project within the Research Fund for Coal and Steel (Project number RFCR-CR-2005-00010).

## References

[1] D. Ristic, M. Schneider, A. Schuster, G. Scheffknecht, J.G. Wünning, Investigation of $NO_x$ formation for flameless coal combustion, in: 7th High Temperature Air Combustion and Gasification International Symposium, Phuket, Thailand, 2008.
[2] H. Stadler, D. Ristic, M. Förster, A. Schuster, R. Kneer, G. Scheffknecht, $NO_x$-emissions from flameless coal combustion in air $Ar/O_2$ and $CO_2/O_2$, Proc. Combust. Inst. 32 (2009) 3131–3138.
[3] R. Backreedy, L. Fletcher, L. Ma, M. Pourkashanian, A. Williams, Modelling pulverised coal combustion using a detailed coal combustion model, Combust. Sci. Technol. 178 (2006) 763–787.
[4] W. Fiveland, C. Latham, Use of numerical modeling in the design of a low-$NO_x$ burner for utility boilers, Combust. Sci. Technol. 93 (1993) 53–72.
[5] H. Kim, Y. Kim, S. Lee, K. Ahn, NO reduction in 0.03–0.2 MW oxy-fuel combustor using flue gas recirculation technology, Proc. Combust. Inst. 31 (2007) 3377–3384.
[6] A. Molina, E. Eddings, D. Pershing, A. Sarofim, Char nitrogen conversion: implications to emissions from coal-fired utility boilers, Prog. Energy Combust. Sci. 26 (2000) 507–531.

[7] A. Williams, R. Backreedy, R. Habib, J. Jones, M. Pourkashanian, Modelling coal combustion: the current position, Fuel 81 (2002) 605–618.
[8] N. Schaffel, M. Mancini, A. Szlek, R. Weber, Mathematical modeling of MILD combustion of pulverized coal, Combust. Flame doi:10.1016/j.combustflame.2009.04.008.
[9] K. Yamamoto, M. Taniguchi, K. Kiyama, J. Matsuda, A study of gasification reactions in pulverized coal combustion, in: Third International Symposium on Advanced Energy Conversion Systems and Related Technologies, RAN2001, Nagoya, Japan, 2001.
[10] P. Jensen, P. Ereaut, S. Clausen, O. Rathmann, Local measurements of velocity temperature and gas composition in a pulverised-coal flame, J. Inst. Energy 67 (1994) 37–46.
[11] D. Toporov, P. Bocian, P. Heil, A. Kellermann, H. Stadler, S. Tschunko, M. Förster, R. Kneer, Detailed investigation of a pulverized fuel swirl flame in $CO_2/O_2$ atmosphere, Combust. Flame 155 (2008) 605–618.
[12] B. Magnussen, The eddy dissipation concept a bridge between science and technology, in: ECCOMAS Thematic Conference on Computational Combustion, 2005.
[13] P. Heil, D. Christ, D. Toporov, M. Förster, R. Kneer, Investigations of a burner for flameless combustion in $CO_2/O_2$ -atmosphere, in: 8th European Conference on Industrial Furnaces and Boilers, 2008.
[14] D. Shaw, X. Zhu, M. Misra, R. Essenhigh, Determination of global kinetics of coal volatiles combustion, in: 23rd Symposium (International) on Combustion, 1990, pp. 1155–1162.
[15] J. Howard, G. Williams, D. Fine, Kinetics of carbon monoxide oxidation in postflame gases, in: 14th Symposium (International) on Combustion, 1973, pp. 975–986.
[16] K. Hsu, A. Jemcov, Numerical Investigation of Detonation in Premixed Hydrogen-air Mixture-assesment of Simplified Chemical Mechanisms, AIAA Paper 2000-2478, Denver, CO, 2000.
[17] D. Ye, J. Agnew, D. Zhang, Gasification of a south australian low-rank coal with carbon dioxide and steam: kinetics and reactivity studies, Fuel 77/11 (1998) 1209–1219.
[18] S. Kajitani, S. Hara, H. Matsuda, Gasification rate analysis of coal char with a pressurized drop tube furnace, Fuel 81 (2002) 539–546.
[19] S. Kajitani, N. Suzuki, M. Ashizawa, S. Hara, $CO_2$ gasification rate analysis of coal char in entrained flow coal gasifier, Fuel 85 (2006) 163–169.
[20] K. Miura, K. Hashimoto, P.L. Silveston, Factors affecting the reactivity of coal chars during gasification and indices representing reactivity, Fuel 68 (1989) 1461–1475.
[21] E. Hampartsoumian, P. Murdoch, M. Pourkashanian, D. Trangmar, A. Williams, The reactivity of coal chars gasified in a carbon dioxide environment, Combust. Sci. Technol. 92 (1993) 105–121.
[22] A. Molina, F. Mondragón, Reactivity of coal gasification with steam and $CO_2$, Fuel 77/15 (1998) 1831–1839.
[23] M. Field, Rate of combustion of size-graded fractions of char from a low-rank coal between 1200 K and 2000 K, Combust. Flame 13 (1969) 237–252.
[24] D. Smoot, D. Pratt, Pulverised-coal Combustion and Gasification Theory and Applications for Continuous Flow Processes, Plenum Press, 1979.
[25] J. Brouwer, M. Heap, D. Pershing, P. Smith, A model for prediction of selective noncatalytic reduction of nitrogen oxides by ammonia, urea, and cyanuric acid with mixing limitations in the presence of CO, in: 26th Symposium (International) on Combustion, 1996, 2117–2124.
[26] P.G. Kristensen, P. Glarborg, K. Dam-Johansen, Nitrogen chemistry during burnout in fuel-staged combustion, Combust. Flame 107 (1996) 211–222.
[27] A. Bose, K. Dannecker, J. Wendt, Coal composition effects on mechanisms governing the destruction of NO and other nitrogenous species during fuel-rich combustion, Energy Fuel. 2 (1987) 301–308.
[28] J.P. Spinti, D.W. Pershing, The fate of char-N at pulverized coal conditions, Combust. Flame 135 (2003) 299–313.
[29] M.U. Alzueta, R. Bilbao, A. Millera, Modeling low-temperature gas reburning. $NO_x$ reduction potential and effects of mixing, Energy Fuel. 12 (1998) 329–338.
[30] M. Mancini, P. Schwöppe, R. Weber, Numerical computation of $NO_x$ formation in MILD combustion of natural gas, in: Computational Combustion 2007, ECCOMAS Thematic Conference, 2007.